Prediction of Inelastic Tensile Strain Capacity of High Performance Fiber Reinforced Composites (FRC) - A Parametric Study

by

Will Hansen, Ph.D., Professor, Department of Building Technology and Structural Engineering, Aalborg University Center (AUC), Sohngårdsholmsvej 57, 9000 Aalborg, Denmark

Prijatmadi Tjiptobroto, Ph.D., Research Associate, Department of Civil Engineering, G. G. Brown Building, The University of Michigan, Ann Arbor, Michigan 48109, USA

Abstract

A model developed by the author's for predicting the inelastic strain capacity of high performance fiber reinforced composites containing high volume fraction of discontinuous fibers was evaluated from a limited experimental program. The system studied was FR-DSP (Densified Small Particle). The DSP mortar has a compressive strength of about 175 MPa. The fresh mortar of densely packed particles and low water to cementitious ratio is particularly suitable for incorporating high volume fraction of fine fibers. In this study short (6 mm) and fine (0.15 mm diameter) steel fibers were used. The fiber contents by volume were 0%, 3%, 6%, 9% and 12%.

The load-deformation response in flexure of the FR-DSP specimens showed that the strain capacity of the brittle DSP mortar was substantially improved, and the major contributor to total strain is the inelastic strain associated with multiple microcracking. At 6% fiber volume the inelastic strain capacity is about 0.13% increasing to about 0.2% at a fiber content of 12%. However the scatter in results was large. Despite this a trend of increasing inelastic strain with increasing fiber content was obtained.

The model predictions were within the range of measured values and showed similar trend with fiber content. More results are needed to validate the proposed model.

Key words: concrete, FRC, inelastic strain, multiple microcracking, tensile strain modeling,.

1. Introduction

In a previous papers /1/ it was demonstrated that the addition of high volume fraction of short and fine steel fibers can lead to an increase in the strain capacity of the composite. A model, based on energy principles, was proposed for predicting the inelastic strain of high performance FRC.

In this paper the model is evaluated and the predictions are compared to inelastic strain data obtained on the DSP (Densified Small Particles) system containing fiber volumes of 0, 3%, 6%, 9%, and 12%. The effect of basic matrix and fiber parameters are studied through parametric modeling. A framework for design purposes is presented.

2. Background

The term inelastic strain as used in this paper is defined as the strain of a high performance fiber reinforced composite (FRC) between the point of first cracking and the starting point of the softening stage. This is illustrated in Figure 1a for a typical high performance FRC, as proposed by Naaman /2/, where the inelastic strain is shown as the strain in region II. The inelastic strain region is characterized by the occurrence of multiple micro-cracking throughout the composite. Even though cracks are present, the term strain can still be used since strain localization has not occurred.

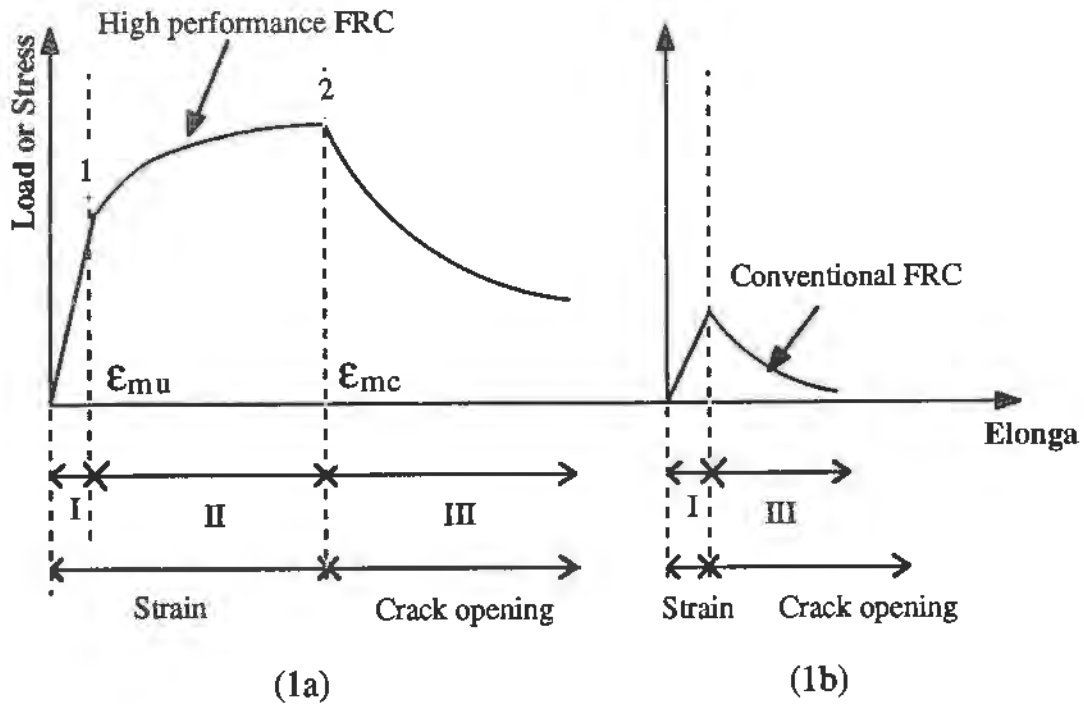

Figure 1. Typical tensile load-elongation response for high performance FRC in Fig.1a , and conventional FRC in Fig.1b.

Region II may not exist in FRC with low fiber volume (i.e. 1-2%).

From the literature there are no models available for predicting the inelastic strain capacity of high performance FRC reinforced with discontinuous fibers. Several analytical models have been proposed to predict the post cracking strength of fiber reinforced composites /2,4,5,6,7,8/. These models are based on the mechanics of composite approach assuming a composite failure by fiber pull-out. However, these models predict the maximum strain capacity obtained from the ratio of maximum post cracking strength over the post-cracking (damaged) modulus of elasticity. Thus an error is obtained due to the non-linearity of the stress-strain response. Only the recoverable strain (Figure 2) can be obtained, not the maximum strain capacity of the composite. In high performance FRC a high degree of non-linearity exists due to multiple microcracking. Thus, the unrecoverable strain may be significant.

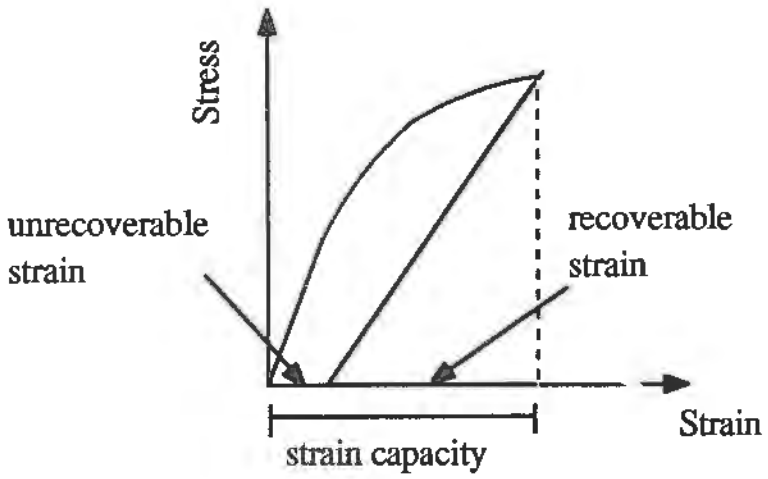

Figure 2. Sketch illustrating the difficulties in using maximum stress results for strain capacity prediction

A model was proposed by Aveston, Cooper, and Kelly (ACK model) /9/ to predict the multiple cracking strain in continuous FRC. This model was derived using energy principles during cracking. In practice, the ACK model has also been used for discontinuous fiber composites by applying correction factors taking into account the orientation of the discontinuous fiber /11,12/. Comparison between the multiple cracking strain prediction of the ACK model and experimental data for fiber reinforced DSP shows that the ACK model is very sensitive to fiber efficiency factor values /12/.

3. Proposed model

The model proposed in this study for predicting the multiple cracking strain (inelastic strain) in discontinuous FRC is derived from energy principles. The following energy changes during cracking were considered in the model derivation :

(1) The increase in the fiber strain energy, ΔU_f, as the result of the crack-bridging action of the fibers.

(2) The frictional energy, ΔU_{fr}, which is the energy absorbed due to the difference in strain (slip) of the fiber and the matrix.

(3) The debonding energy, U_{db}, which is the energy required to destroy the elastic bond at the fiber-matrix interface.

(4) The change in external work, $\Delta W_{external}$, due to elongation of the fiber as the result of the crack-bridging action of the fibers.

The energy balance equation for the multiple cracking region is:

$$\Delta W_{external} = \Delta U_f + \Delta U_{fr} + U_{db} \tag{1}$$

After evaluating each energy term and substituting them into equation 1, the following equation is obtained for predicting the multiple cracking strain, ε_{mc}, (Fig. 1a) as derived in reference /1/:

$$\varepsilon_{mc} = \varepsilon_{mu} - \frac{3}{8}\frac{\tau_f L_f}{E_f r} + \left[\frac{\tau_f L_f}{E_f r}\left[\frac{\tau_f L_f}{E_f r}\left(\frac{9}{64} + \frac{11}{24}\frac{E_f V_f}{E_c^*}\right) - \varepsilon_{mu}\left(\frac{3}{4} + \frac{1}{4}\frac{E_f V_f}{E_c^*}\right)\right] + \varepsilon_{mu}^2\left(1 - \frac{1}{2}\frac{E_f V_f}{E_c^*}\right) + \frac{2 V_f G_{II}}{E_c^* r}\right]^{1/2} \tag{2}$$

where ε_{mu} is the elastic strain capacity of the composite. This value increases with fiber content in FRC containing high fiber volume fraction such as the FR-DSP system investigated in this study. A model for predicting the elastic strain capacity of FRC with high fiber volume fraction discontinuous fibers has been developed previously by the authors /13,14/.

τ_f , is the frictional interface stress between fiber and matrix at the end of the multiple cracking stage (i.e. end of region II). In the derivation of equation 2 , τ_f is assumed to be constant throughout the fiber embedment length. This implies that there is no elastic bond remaining between fiber and matrix at this point.

L_f is the fiber length, r is the fiber radius, E_f is the fiber modulus, and E_c^* is the modulus of elasticity of the cracked composite (i.e. elastic modulus in the multiple cracking stage). Approximation of the post-cracking modulus is obtained from the slope of the unloading-reloading branch of the load-deformation curve near the peak-load (i.e. end of region II) as shown in Figures 13 and 14. V_f is the relative volume fraction of fibers. G_{II} is the fracture energy in shear mode between fibers and matrix. This parameter is discussed in more detail in section 6.3.2.

Rewriting equation 2:

$$\varepsilon_{mc} = \varepsilon_{mu} - \frac{3}{8} A + \sqrt{A\left[A\left(\frac{9}{64}+\frac{11}{24}B\right) - \varepsilon_{mu}\left(\frac{3}{4}+\frac{1}{4}B\right)\right] + \varepsilon_{mu}^2\left(1-\frac{1}{2}B\right) + \frac{2V_f G_{II}}{E_c^* r}} \qquad (3)$$

where : $$A = \frac{\tau_f L_f}{E_f r} \qquad (4)$$

and $$B = \frac{E_f V_f}{E_c^*} \qquad (5)$$

Term A represents the influence of the stress transfer property (τ_f) and the basic fiber properties namely the length, modulus of elasticity, and the radius of the fiber. Term B represents the ratio of the modulus of elasticity of the cracked-composite if it was reinforced with continuous fibers ($E_f V_f$) to that of a composite of same composition reinforced with discontinuous fibers (E_c^*). The value of B will be less than one.

The multiple cracking strain (ε_{mc}) represents the strain at the end of the multiple cracking stage and it is, therefore, the sum of both the elastic strain (ε_{mu}) and the inelastic strain as seen from Figure 1a. Thus, the inelastic strain can be obtained from equation 3 by subtracting the elastic strain, ε_{mu}, from equation 3.

An approximation and simplification of equation 3 can be obtained by deleting the terms that contain the matrix cracking strain

$$\varepsilon_{mc} \approx \varepsilon_{mu} + A\left[\sqrt{\frac{9}{64}+B\left(\frac{11}{24}+\frac{2G_{II}}{A\tau_f L_f}\right)} - \frac{3}{8}\right] \qquad (6)$$

It can be shown that the predictions using equation 6 are close to predictions according to equation 3 /13/. However, equation 6 is more practical.

4. Critical fiber volume fraction

The first step in applying equations 3 or 6 is to check whether multiple cracking can be expected to occur. The critical fiber volume fraction required to achieve multiple cracking can be calculated from the following equation from reference /3/ using energy principles:

$$V_{ef\text{-}cr} = \frac{\gamma_m + \sqrt{\gamma_m^2 + C}}{C} \tag{7}$$

$$C = 2\,\gamma_m + \frac{L_f}{r}\left(\frac{11}{48}\,\tau_f^2\,\frac{L_f^2}{E_f\,r}\right) \tag{8}$$

where $V_{ef\text{-}cr}$ is the critical effective fiber volume fraction and γ_m is the matrix surface energy ($^1/_2\,G_m$). For fibers randomly distributed within the matrix, the number of fibers effectively bridging a crack is half the total number of fibers that may intercept the crack plane. Therefore, the critical nominal fiber volume fraction, $(V_f)_c$, is twice the effective fiber volume fraction:

$$(V_f)_c = 2\,V_{ef\text{-}cr} \tag{9}$$

Equation 7 was derived from energy principles assuming that:

$$E_{1\text{-}2} = E_2 \tag{10}$$

where $E_{1\text{-}2}$ is the energy required to open the first microcrack during multiple cracking stage from point 1 to point 2, which is the end of the multiple cracking stage. $E_{1\text{-}2}$ is the right hand side of equation 1. E_2 is the energy required to form a new microcrack where:

$$E_2 = G_m V_m + \Delta U_{f\text{-}mu} - \Delta U_m \tag{11}$$

$G_m V_m$ is the total fracture energy of the matrix which is the energy required to create a new surface, where G_m is the matrix fracture energy, and V_m is the matrix volume fraction.

$\Delta U_{f\text{-}mu}$ is the increase in the fiber strain energy as the result of the bridging action at the end of region I.

ΔU_m is the decrease in the matrix strain energy since the strain in the matrix at the crack face will be reduced to zero.

A detailed discussion on critical fiber volume fraction and multiple cracking can be found in reference /3/. As an example, the predicted critical fiber volume are shown graphically in Figures 3 and 4 respectively for FR-DSP and a typical FRC . The input

parameters used in equations 7 and 8 are shown in Table 1. Input parameters such as compressive strength, modulus of elasticity and fracture energy for the FR-DSP system was measured in an earl;ier study by one of the authors /12/. Compressive strength and elastic modulus was obtained from cylinders of dimensions 45 mm by 90 mm (height). The fracture energy of the DSP mortar matrix, G_m, was determined from flexure tests, (centerpoint loading) using notched beams of dimensions 50 mm by 50 mm by 500 mm.

The frictional stress τ_f was estimated. A more detailed discussion on this parameter is found in section 6.3.1.

All input values to the ordinary FRC shown in Table 1 are estimates. The predicted critical fiber volume for occurrence of multiple microcracking for ordinary FRC was found to be about 15%. Thus multiple microcracking will not occur in this case since the maximum achievable fiber content for ordinary FRC is about 1-3%.

Table 1. Input parameters and characteristics of FR-DSP and ordinary FRC

Materials	Fiber reinforced DSP	Ordinary FRC
Matrix:		
Compressive strength	175 MPa	20 MPa
Modulus of elasticity	49,100 MPa	21,000 MPa
Frictional stress (τ_f)	5 MPa	1 MPa
Fracture energy (G_m)	120 N/m	20 N/m
Interface fracture energy (G_{II})	120 N/m	2.5 N/m
W/C ratio	0.18	0.4 - 0.6
Steel Fiber:		
Modulus of elasticity	200,000 MPa	200,000 MPa
Length	6 mm	25 mm
Diameter	0.15 mm	0.5 mm

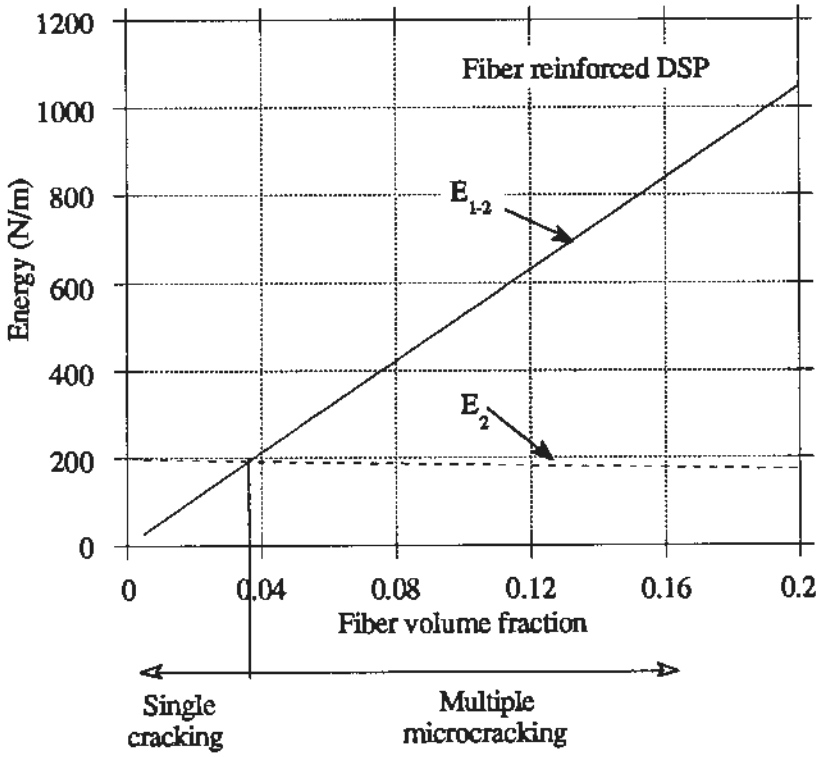

Figure 3 . The critical fiber volume fraction for fiber reinforced DSP.

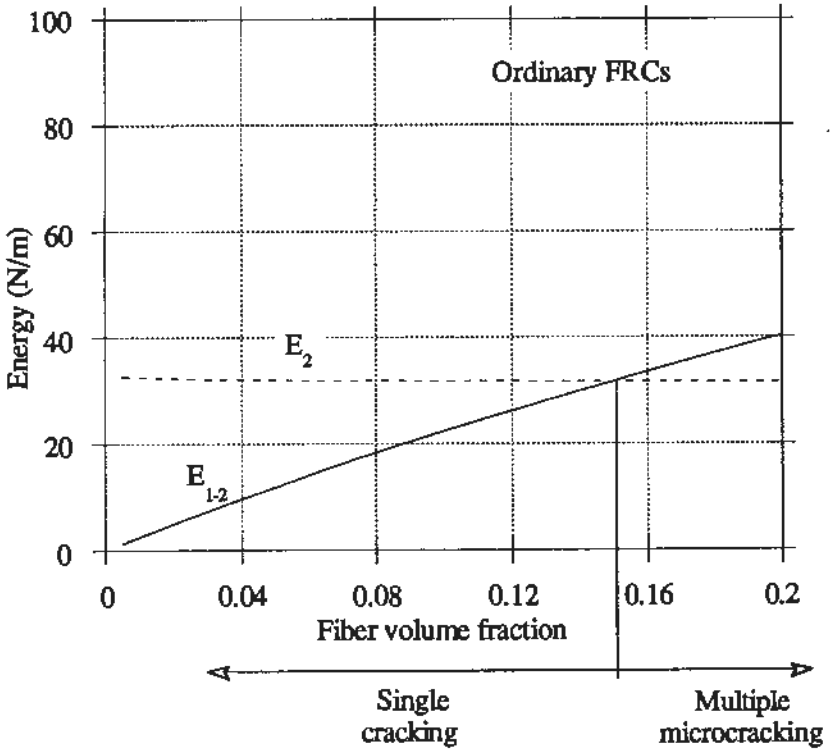

Figure 4 . The critical fiber volume fraction for ordinary FRC.

5. Experimental

Materials, mixing, and curing are the same as those in references /3,12 and 13/.

The data obtained from experiments includes the inelastic strain, modulus of elasticity at the end of the multiple cracking region, and crack observations.
Beam of dimensions 50 mm by 50 mm by 500 mm were tested in flexure (third point loading) as illustrated in Figure 5.

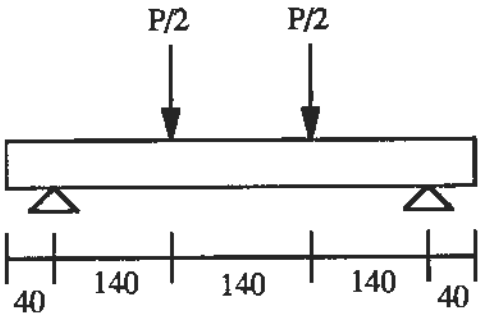

Figure 5. Flexure test loading arrangement.

Three test set-ups were used in the experiments. In the first set-up four strain gauges were placed at the mid-section of the beam; two were placed on the compression side while the other two were placed on the tension side (Figure 6). Tests using this set-up were carried out for fiber volume fractions of 0, 3%, 6%, 9%, and 12%. Accurate measurements of the inelastic strain values can be obtained from this set-up.

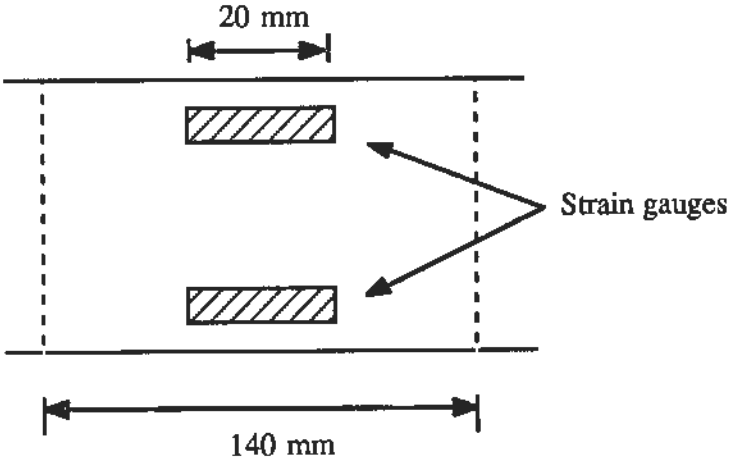

Figure 6. Strain gauge arrangement for inelastic strain measurements.

The second set-up was designed to gain some insight on the formation of microcracks in the inelastic region. Strain values at different locations along the constant moment

length of 60 mm were used (Figure 7). Tests were carried out for fiber volumes of 6% and 12%.

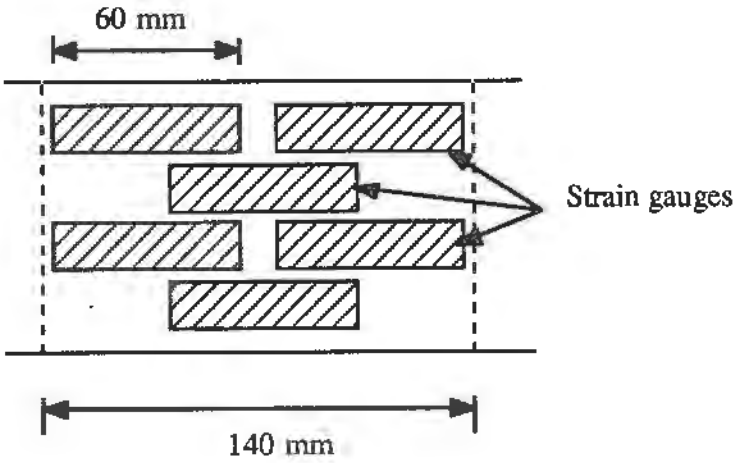

Figure 7 . Strain gauge arrangement for crack observations on maximum tensile moment section of beam.

The third set-up (Figure 8) was used in obtaining the modulus of elasticity of the composite at the end of the inelastic region. For these tests the load was increased up to peak load before two un-loading and re-loading cycles were performed. The modulus of elasticity of the composite was obtained by comparing the initial slope of the elastic range with the un-loading re-loading slope.

Also obtained from this test were the crack patterns and crack width from observations using optical microscopy. Investigations were carried out for fiber volumes 6% and 9%.

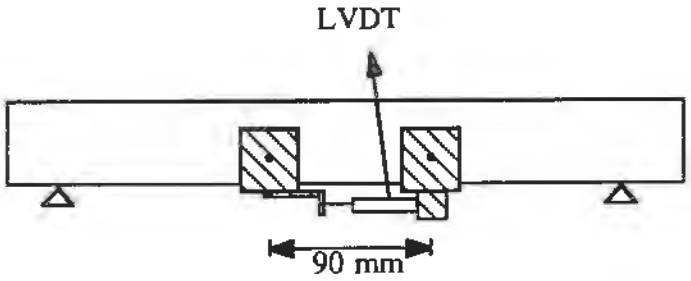

Figure 8. Test set-up for post-cracking modulus prediction

6. Results and Discussion

6.1 Tensile strain hardening

A typical load-tensile strain response in flexure for different fiber volume fractions is shown in Figure 9.

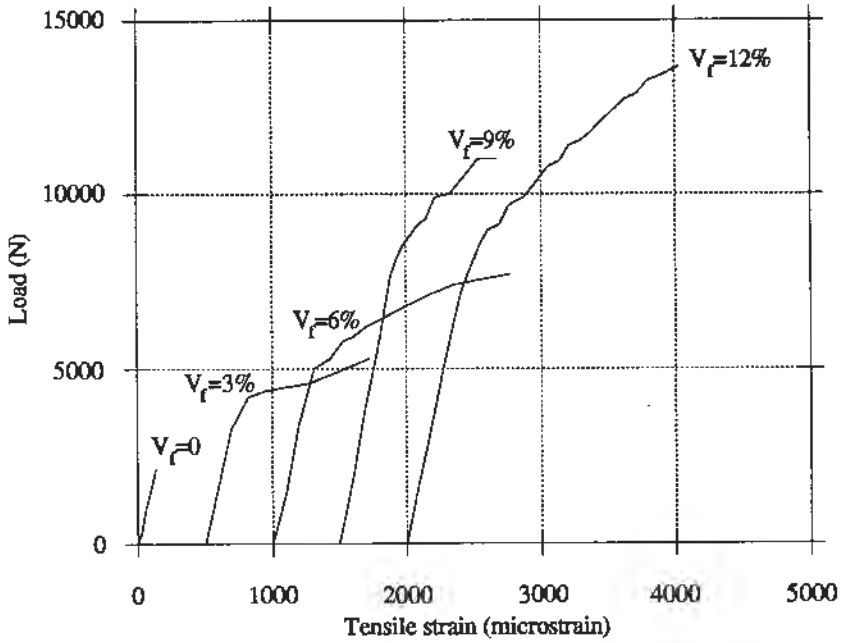

Figure 9. Typical load-tensile strain response of DSP with different fiber volumes.

The inelastic region, shown in Figure 9, is the "tensile strain hardening" region which substantially improves the performance of the composite. Improvements in both the load-carrying capacity and tensile strain capacity are evident. Therefore the term "tensile strain hardening" as known from steel. A major part of the improvement in tensile strain capacity is attributed to the increase in the inelastic strain. The inelastic strain values can be obtained by subtracting from the maximum-load strain value the elastic strain. Shown in Figure 10 are the inelastic strains obtained for the FR-DSP specimens for the different fiber volumes.

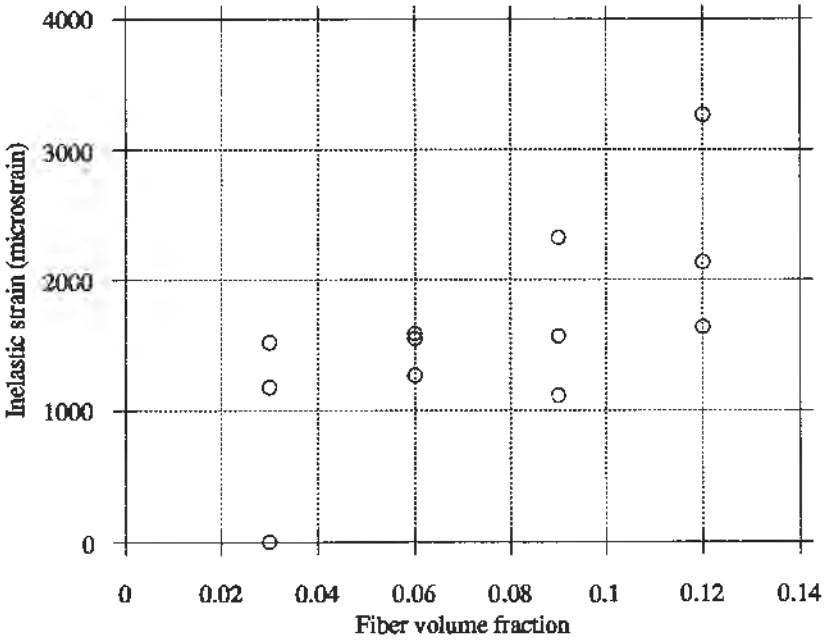

Figure 10 . Measured inelastic strain values for FR-DSP.

Although the variation in the results is large, there is a clear trend of increasing inelastic strain with fiber content.

6.2 Crack observations

The increase in the inelastic strain was accompanied by the formation of microcracks. These microcracks were not visible up to maximum load. In this investigation the formation of microcracks was detected from strain gauge readings using a test set-up shown in Figure 7, and from optical microscopy examination of unloaded beams after reaching peak load. It was found that the number of cracks increased with increasing fiber content. On the average there were about 8 cracks for V_f of 12%, and 4 to 5 cracks for V_f of 9%, and 3 to 4 cracks for V_f of 6%. Figures 11 and 12 show typical crack patterns that were observed for the FR-DSP system.

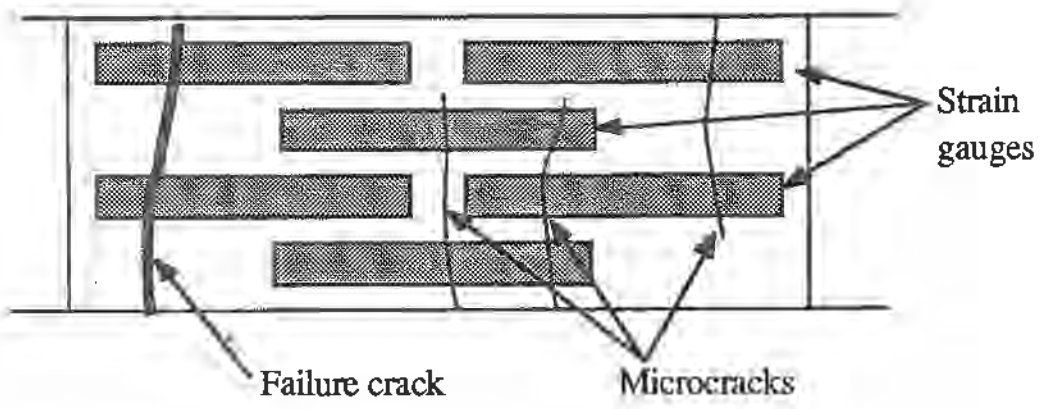

Figure 11. Typical tensile crack pattern obtained on FR-DSP containing 6% by volume fibers.

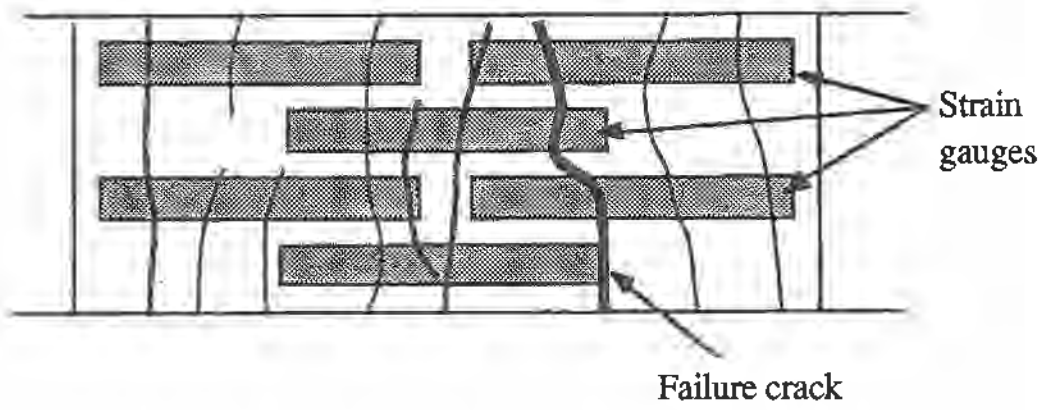

Figure 12. Typical tensile crack pattern obtained on FR-DSP containing 12% by volume fibers.

The slope of the unloading-reloading response can be compared to the initial slope to approximate the composite modulus in region II. The load-strain response including that of the unloading-reloading cycles is shown in Figures 13 and 14 for V_f of 6% and 9% respectively. For V_f of 6% the percentage found was 40%, while it was 32% for V_f of 9%. The assumption used in model predictions of inelastic strain that the composite modulus in region II is 35% of the initial elastic modulus seems to be acceptable based on the results for V_f of 6% and 9%.

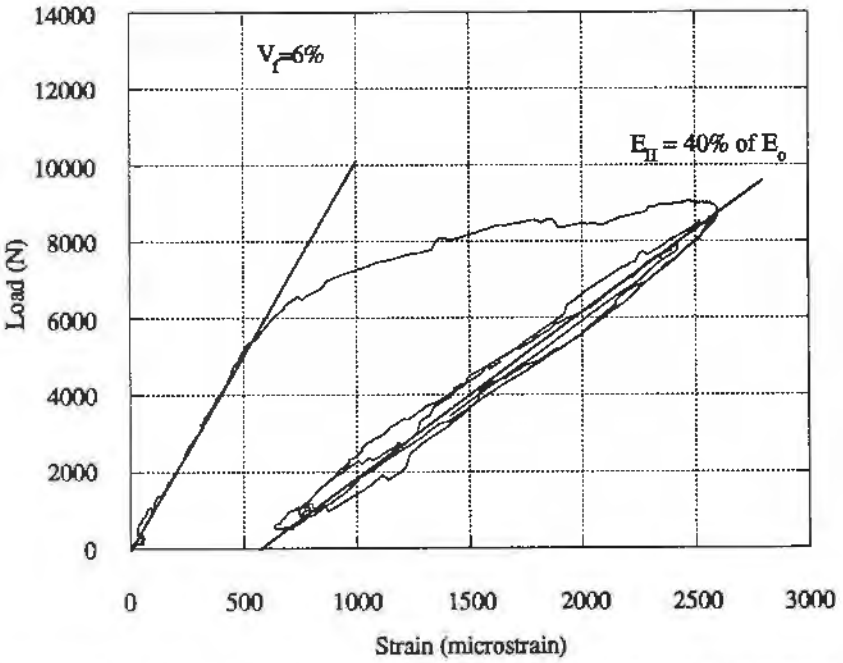

Figure 13. Approximation of post-cracking modulus of FR-DSP from the slope of the unloading-reloading response for V_f of 6%.

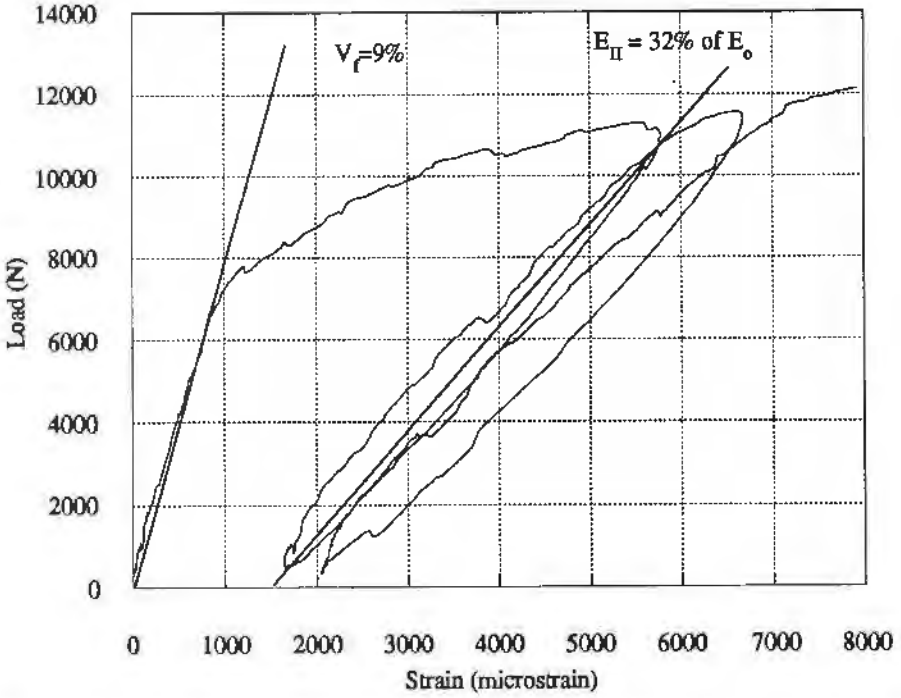

Figure 14. Approximation of post-cracking modulus of FR-DSP from the slope of the unloading-reloading response for V_f of 9%.

In conclusion, combining the results from crack observations and load-strain response in the multiple cracking region, one can associate the increase in the inelastic strain with

the increase in the number of microcracks. And the presence of high volume fraction of fibers prevents the occurrence of strain localization in the composite.

6.3 Evaluation of the model using the FR- DSP data

Three important input parameters needed for the inelastic strain modeling are: (1) the interfacial shear strength τ_f; (2) the modulus of elasticity in the cracking stage, E_c^*; and (3) the fracture energy in the shearing mode, G_{II}. Parameters 1 and 3 are difficult to obtain from experiments. In this study these values were estimated.

6.3.1. Interface frictional stress, τ_f.

A value of 10 MPa was assumed and used as input to the model. This value is much higher than that of an ordinary strength cement-based matrix. However, a shear strength of 10 MPa is not unreasonable since it corresponds to only 5.7 % of the compressive strength of the DSP matrix of 175 MPa. Moreover, the DSP matrix has a low water to cementitious ratio and high percentage of microsilica which will improve the microstructure of the fiber-matrix interface. The matrix microstructure in the vicinity of the fiber is very different from that of the bulk. In ordinary FRC this effect is well established and is known as the transition zone effect. The transition zone, which is approximately 10-20 μm away from the fiber surface, is associated with bleeding of water around the fibers and inefficient packing of cement particles. The bleeding of water will result in flaws and a higher relative amount of reaction products of calcium hydroxide. These two sources of weakness at the interface is minimized in the DSP matrix because of the low water-cementitious ratio, dense particle packing, and diminished quantity of calcium hydroxide due to the pozzolanic reaction with microsilica. This will increase the bond strength significantly according to Bentur et. al. /15-18/ and Wei et.al. /19/.

6.3.2. Fracture energy in the second mode (G_{II}).

It is the energy required to destroy the elastic bond between the fiber and the matrix. Not much information is available to estimate the magnitude of G_{II}. Different values of G_{II} were therefore used in the model calculations; 60 N/m, 120 N/m and 180 N/m. These values were chosen around the measured value of fracture energy (G_m=120 N/m) in mode I, obtained from tests on notched-beam specimens. In general, G_{II} is expected to be larger than G_I since more energy is required to fracture a material in a shearing mode than in a tensile/opening mode. From the literature, it has been observed that the critical stress intensity factor in the second mode (K_{IIc}) is larger than that in the first mode (K_{Ic}). The ratio of K_{IIc} to K_{Ic} reported in the literature ranges from 1.5 to 1.8 /20 - 22/.

Having discussed the necessary input parameters, the model, as given by equation 3 (or approximated by equation 6), can be evaluated. The predictions of inelastic strain for different fiber volume fractions and G_{II} values are compared to experimental data in Figure 15. The model seems to predict results well for G_{II} values in the range of 120-180 N/m.

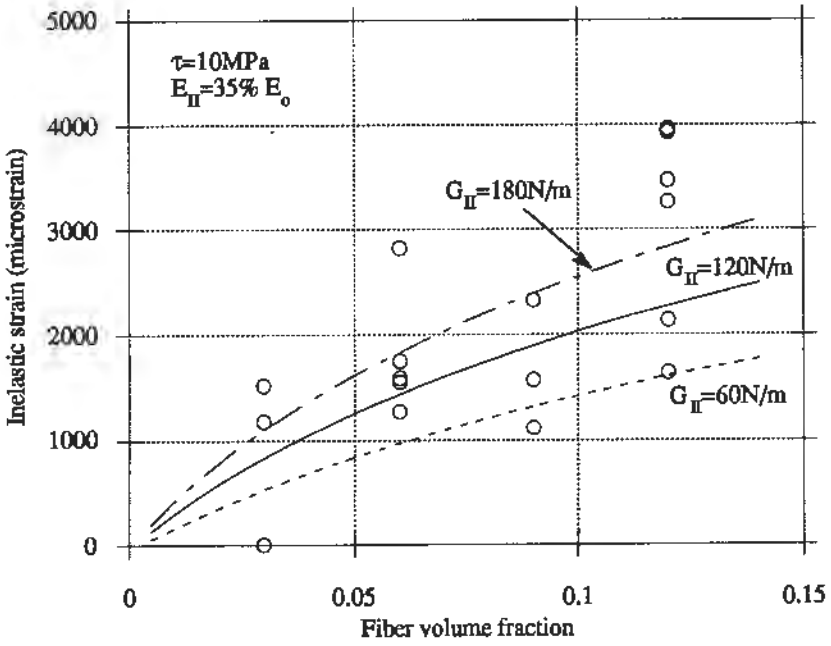

Figure 15. Comparison between predicted inelastic strain values and experimental data for different values of G_{II} for FR-DSP.

A realistic value of G_{II} for the DSP matrix is expected to be between 120 N/m and 180 N/m, (i.e. larger than the fracture energy in the opening mode since the microstructure of the fiber-matrix interface has been significantly improved by particle densification and low water-cementitious ratio).

6.4 Parametric modeling:

Parametric modeling was carried out by varying important input parameters to the model. Modeling was done for the case of elastic and frictional resistance (case 1), and for the case of frictional resistance only (case 2). Case 1, where the debonding energy plays an important role, applies to composites with high bond strength such as DSP composites, whereas case 2 is more applicable to ordinary FRC.

6.4.1 Effect of fiber length on inelastic strain from model predictions

This effect is shown in Figure 16 for case 1 for fiber lengths of 6 mm, 12 mm, and 25 mm. The effect of fiber length is not very straightforward. It seems to depend on the fiber volume.

For case 2, the effect of fiber length is more straightforward as shown in Figure 17. In this case the fiber length has a pronounced effect on the inelastic strain. Longer fibers will result in greater inelastic strain at any fiber volume. However, the total inelastic strain in this case is lower than that where the debonding energy is taken into consideration. This is as expected.

For short fibers, such as the 6 mm steel fibers used in FR-DSP, the inelastic strain is negligible at low fiber volume.

For systems with no elastic bonding and low values of τ_f the inelastic strain will be even less. For an L_f value of 6 mm the inelastic strain is zero (Figure 18). And high fiber volumes will be needed to achieve multiple microcracking. For a fiber length of 25 mm, a fiber content of about 5% is needed to achieve an inelastic strain of 350 microstrain.

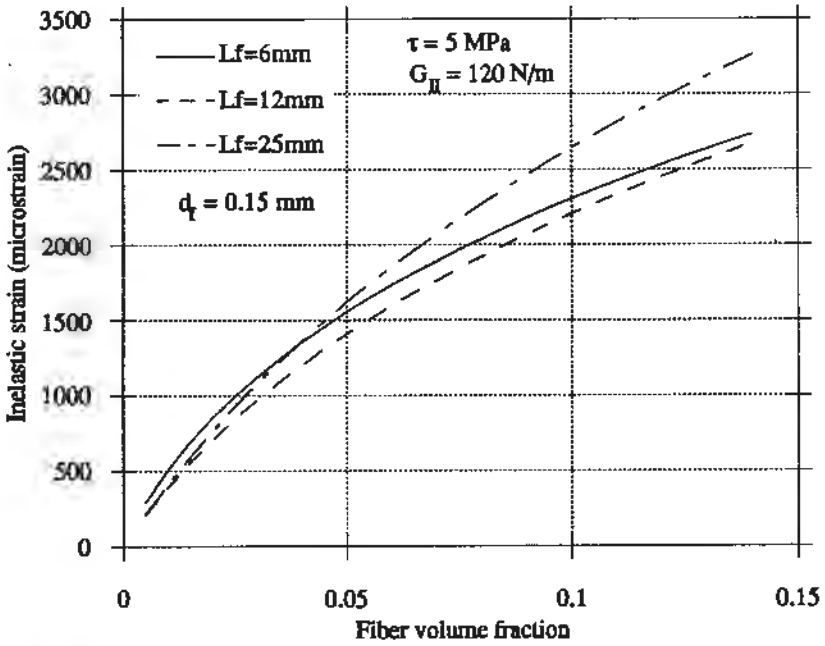

Figure 16. Model predictions for case 1 of effect of steel fiber length on inelastic strain in FR-DSP.

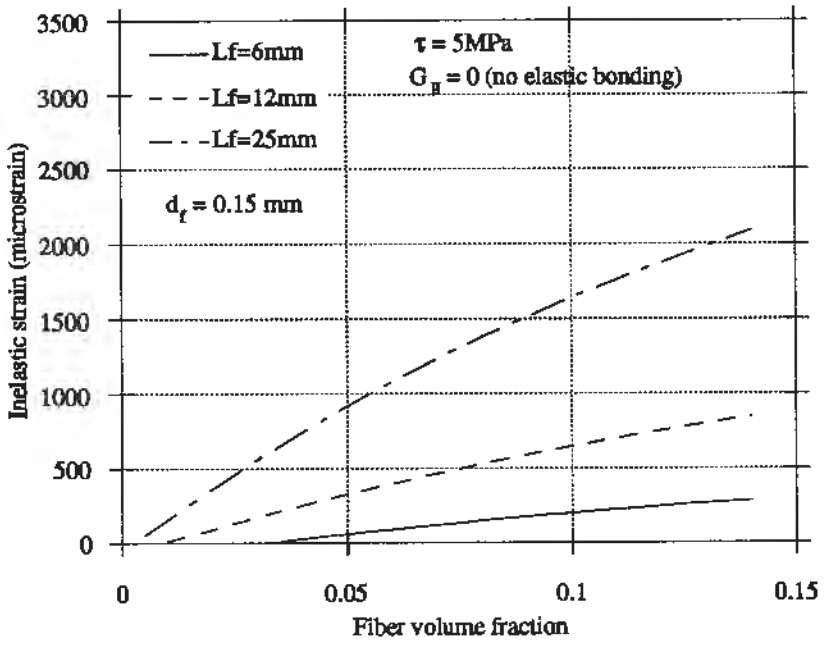

Figure 17. Model predictions for case 2 of effect of steel fiber length on inelastic strain in FR-DSP.

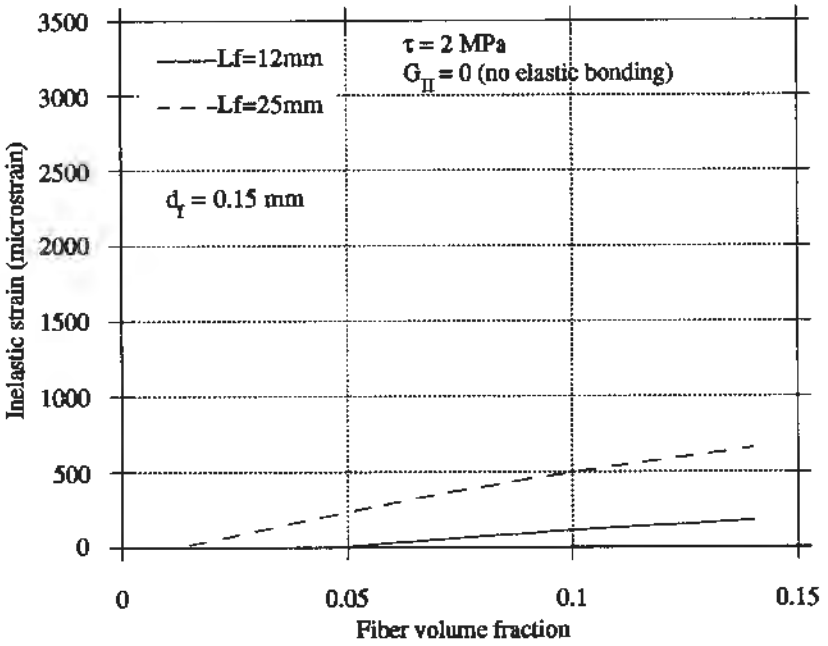

Figure 18. Model predictions for case 2 of effect of steel fiber length on inelastic strain in ordinary FRC where τ_f is small.

6.4.2 Effect of fiber diameter on inelastic strain from model predictions

The effect of fiber diameter on inelastic strain for case 1 is shown in Figure 19 for fiber diameters of 0.015 mm, 0.15 mm, and 0.5 mm. The model predicts that inelastic

strain increases with decreasing fiber diameter. This is what one would expect from considerations of fiber spacing. The same trend is predicted by the ACK model for continuous fibers.

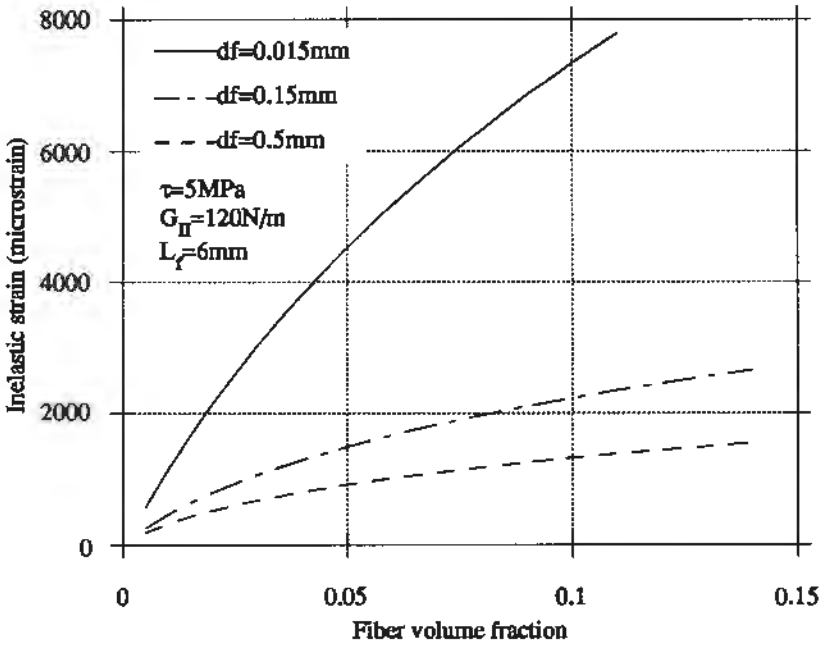

Figure 19. The effect of steel fiber diameter and fiber volume on inelastic strain of a high strength FRC from model predictions.

However, the risk of having fiber breakage will also increase with decreasing fiber diameter. From Figure 19 composites incorporating fibers with a diameter of 0.015mm will be capable of reaching a strain value of about 8000 microstrain (0.8%) at about 12 % fiber volume. Although the predictions are not practical at present, because of problems in mixing small diameter fibers at volumes of 1% or greater, they illustrate that great gains in composite behavior may be achieved by using small diameter fibers.

If the fibers are made from steel with a yield strain of about 2000 microstrain (0.2%), it is clear that the fibers in the composite will yield although the fiber strain is much smaller than the composite strain due to the occurrence of multiple cracking. If the fibers are brittle, such as carbon fibers, it is likely that they will break. Thus, if small diameter fibers are used, it is important to use fibers made from materials which exhibit high values of both plastic deformation and tensile strength. The tensile strength of the steel fibers used in this study is reported to be 2950 MPa.

The effect of fiber diameter on inelastic strain for case 2 is shown in Figure 20. The same trend is predicted as before (case 1). However the strain values are smaller. Steel

fibers of 0.5 mm diameter do not result in multiple microcracking in a weak FRC in which there is no elastic bond.

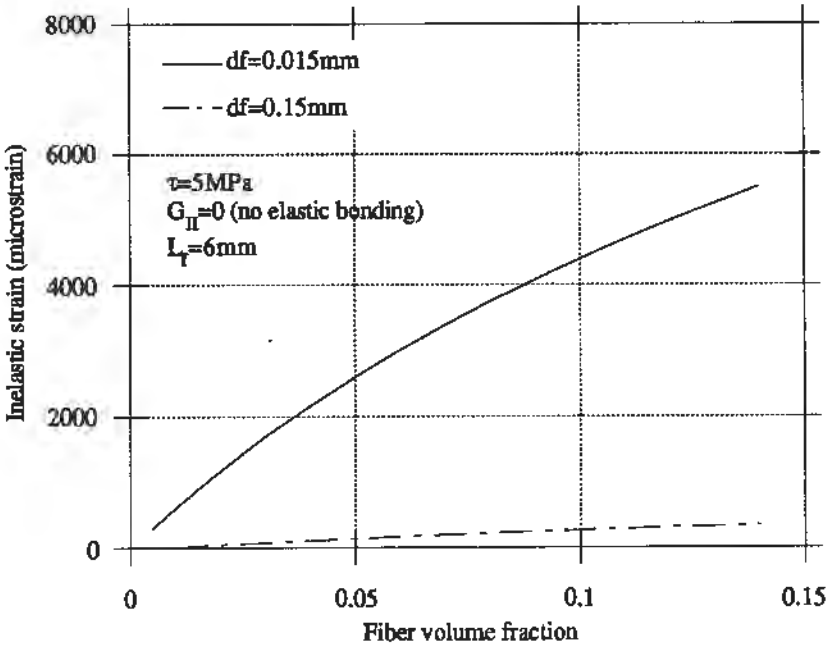

Figure 20. Model predictions of effect of fiber diameter on inelastic strain for case 2 (i.e. without elastic bonding), and a τ value of 5 MPa.

For systems without elastic bonding and low values of τ the inelastic strain will be even more reduced. For a fiber diameter of 0.15 mm the inelastic strain is almost negligible (Figure 21).

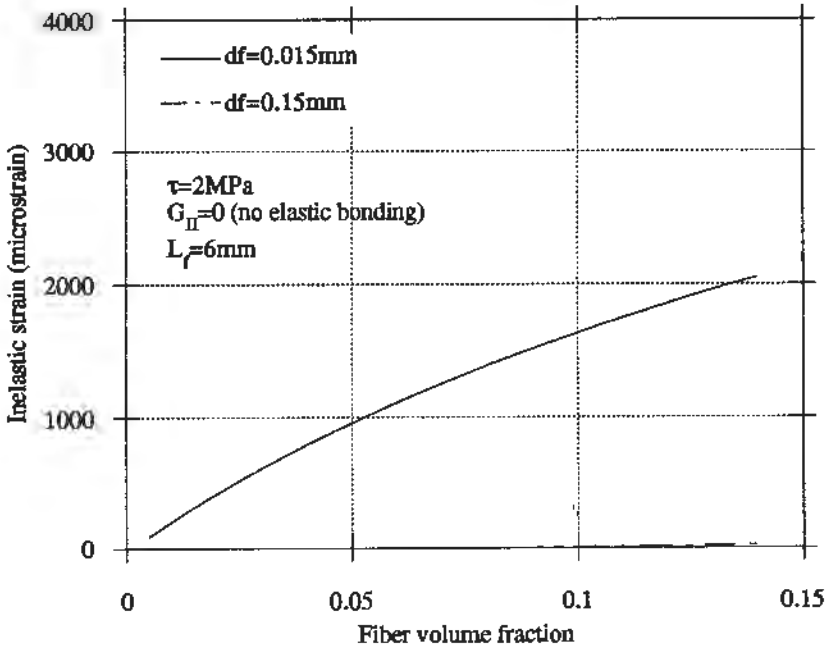

Figure 21. Model predictions of effect of fiber diameter on inelastic strain for case 2 (i.e. without elastic bonding), and a τ value of 2 MPa.

6.4.3 Effect of fiber modulus on inelastic strain from model predictions

The modulus of elasticity of the fibers will have a major influence on the inelastic strain capacity according to the proposed model. This is illustrated in Figure 22 for case 1 and Figure 23 for case 2 . The FRC system in Figures 22 and 23 resembles a FR-DSP system with and without elastic bonding.

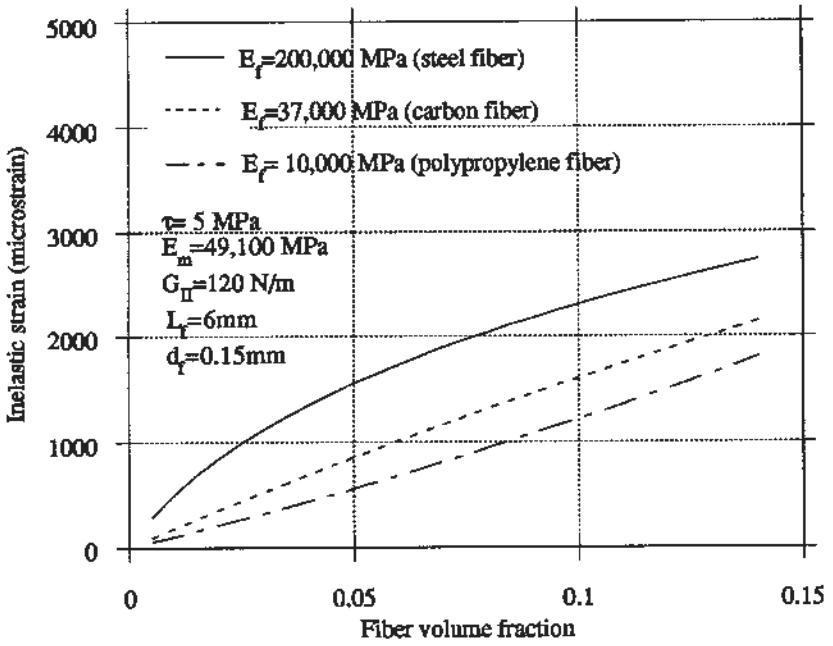

Figure 22. The predicted effect of modulus elasticity of fibers on inelastic strain for a G_{II} value of 120N/m.

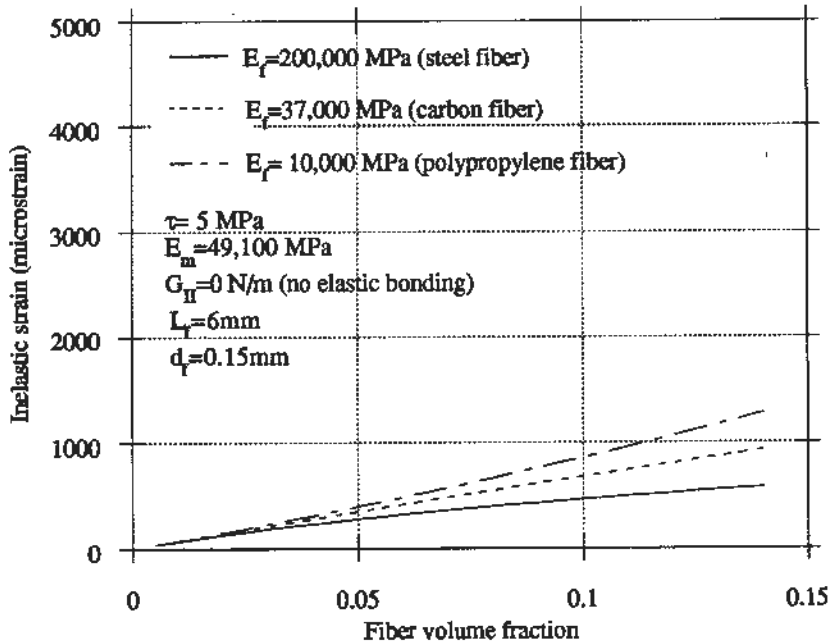

Figure 23. The predicted effect of modulus elasticity of fibers on inelastic strain without elastic bonding.

As evident from Figures 22 and 23, the trend is reversed from the case with debonding to the case without debonding. In case 1 (Figure 22) the inelastic strain will increase with increasing fiber modulus.

When there is no elastic bonding (i.e. case 2) only low level of load (stress) can be applied to the fibers. In this case fibers with low modulus are more effective for storing strain energy since low levels of load (stress) is sufficient to stretch the fibers. However, with the presence of elastic bonding, higher load (stress) levels can be applied, which means that fibers with high values of modulus of elasticity will become more effective in storing elastic energy and thus more effective with respect to improvement in tensile strain capacity.

6.4.4 Summary of parametric modeling

Table 2 summarizes the findings from the parametric study:

Table 2. Effect of input parameters on inelastic strain predictions.

Input Parameter	Elastic bonding and frictional resistance ($G_{II}\neq0$)	Frictional resistance only ($G_{II}=0$)
Interface shear stress (τ)	ε_{in} is a function of G_{II}	ε_{in} increases as τ increases
Modulus elasticity of fiber (E_f)	ε_{in} increases as E_f increases	ε_{in} decreases as E_f increases
Fiber length (L_f)	ε_{in} is a function of V_f	ε_{in} increases as L_f increases
Fiber diameter (d_f)	ε_{in} increases as d_f decreases	
Note : ε_{in} always increases with increasing G_{II} and V_f ε_{in} for $G_{II}\neq0$ is always greater than that for $G_{II}=0$		

7. Conclusions

1. Major improvements were obtained in tensile strain capacity of FR-DSP by reinforcing the brittle mortar with high volumes (3% to 12%) of short and fine steel fibers. The major contributor to overall strain capacity was the inelastic strain due to multiple microcracking. At a fiber volume of 6% the inelastic strain was about 1000 μm (i.e. 0.1%) increasing to about 2000 μm at 12 % fiber volume. However large scatter was obtained in these results.

2. Model predictions of inelastic strain were within the range of measured values and agreed with the trend of increasing strain with fiber content. More work is needed to validate the model.

3. A parametric study showed that inelastic strain capacity of FRC is significantly affected by the interface properties such as debonding energy and interface frictional stress as well as fiber properties, such as modulus of elasticity, fiber length and fiber diameter.

Acknowledgements:

This research was supported by a grant from the National Science Foundation to the NSF Center for Advanced Cement-Based Materials (Northwestern - 0830-350-B600-UM). The work described is part of a thesis written by Prijatmadi Tjiptobroto in partial fulfillment of the requirements for a Ph.D. degree. The authors would like to thank the Cement and Concrete Laboratory (CBL) of Aalborg Portland for use of their facilities and technical support. The authors would like to thank Messrs. H.H. Bache and B. Aarup from CBL for their help.

8. References:

/1/ Tjiptobroto, P. and Hansen, W.,"A model for predicting the inelastic strain capacity of high performance FRC containing discontinuous fibers", submitted for publication in ACI Materials Journal.

/2/ Naaman, A.E., "High Performance Fiber Reinforced Cement Composites", in Concrete Structures for the Future, IABSE Symposium, Paris-Versailles 1987, pp. 371-376.

/3/ Tjiptobroto, P., and Hansen, W.,"Tensile strain hardening and multiple cracking in cement-based composites reinforced with discontinuous fiber", in press, ACI Materials Journal.

/4/ Naaman, A.E., Moavenzadeh, F., and McGarry, F.,"Probabilistic analysis of fiber reinforced concrete", Journal of Engineering Mechanics Division, ASCE, Vol. 100, No. EM2, April 1974, pp. 397-413.

/5/ Swamy, R.N., and Mangat, P.S.,"A theory for the flexural strength of steel fiber reinforced concrete", Cement and Concrete Research, Vol.4, 1974, pp. 313-325.

/6/ Swamy, R.N., Mangat, P.S., and Rao, C.V.S.K.,"The mechanics of fiber reinforcement of cement matrices", An International Symposium : Fiber Reinforced Concrete, Publication SP-44, American Concrete Institute, Detroit, 1974, pp. 1-28.

/7/ Li, V.C., Wang, Y., Backer, S., ,"A micromechanical model of tension-softening and bridging toughening of short random fiber reinforced brittle matrix composites", in press, Journal of Mechanics and Physics of Solids, April, 1990.

/8/ Wang, Y., Backer, S., Li, V.C.,"A statistical tensile model of fibre reinforced cementitious composites", Composites, Vol. 20, No. 3, May 1989, pp. 265-274.

/9/ Aveston, J., Cooper, G.A., Kelly, A.,"Single and multiple fracture. The properties of fibre composites", Conference Proceedings of National Physical Laboratory, IPC Science and Technology Press Ltd.,1971, pp.15-24.

/10/ Proctor, B.A.,"The stress-strain behavior of glass-fibre reinforced cement composites", Journal of Materials Science, Vol. 21, 1986, pp 2441-2448.

/11/ Laws, V.,"Stress/strain curve of fibrous composites", Journal of Materials Science Letters 6, 1987, pp 675-678.

/12/ Tjiptobroto, P.,"Tensile strain hardening of high performance fiber reinforced cement-based composites", Ph.D. dissertation, University of Michigan, Ann Arbor, 1991, 209 pp..

/13/ Tjiptobroto, P., and Hansen, W.,"A model for predicting the elastic strain of FRC containing high volume fractions of discontinuous fibers", in press, ACI Materials Journal.

/14/ W. Hansen, P. Tjiptobroto,"An energy based model for predicting the elastic tensile strain capacity of high performance Fiber Reinforced Composites (FRC)," Nordic Concrete Research, 1991, no. 10, pp. 48 - 67.

/15/ Bentur, A., Diamond, S., and Mindess, S.,"Cracking processes in steel fibre reinforced cement paste", Cement and Concrete Research, Vol. 15, No. 2, 1985, pp. 331-342.

/16/ Bentur, A., Diamond, S., and Mindess, S.,"The microstructure of the steel fibre-cement interface", Journal of Materials Science, Vol. 20, No. 10, 1985, pp. 3610-3620.

/17/ Bentur, A.,"Fiber-Reinforced Cementitious Materials", in "Materials Science of Concrete", edited by J.P. Skalny, American Ceramic Society, Westerville, Ohio, 1990, pp. 223-283.

/18/ Bentur, A.,"Interfaces in fibre reinforced cements", in "Bonding in Cementitious Composites", Materials Research Society Symposium Proceedings, edited by S. Mindess and S.P. Shah, Materials Research Society, Pittsburgh, Pennsylvania, Vol. 114, 1988, pp. 133-144.

/19/ Wei, S., Mandel, J.A., and Said, S.,"Study of the interface strength in steel fiber-reinforced cement-based composites", ACI Materials Journal, Proceedings V. 83, No. 4, 1986, pp. 597-605.

/20/ Davies, J, Morgan, T.G., and Yim, A.W.,"The finite element analysis of specimens giving a mode II type of failure", in Fracture Toughness and Fracture Energy of Concrete edited by F.H. Wittmann, Elsevier Science Publisher, 1986, pp. 209-212.

/21/ Izumi, M., Mihashi, H., and Nomura, N.,"Fracture toughness of concrete for mode II", in Fracture Toughness and Fracture Energy of Concrete edited by F.H. Wittmann, Elsevier Science Publisher, 1986, pp 347-354.

/22/ Xu, S., Chen, S., and Zhao, G.,"Development of fracture mechanics of concrete in China", in Fracture Toughness and Fracture Energy of Concrete edited by F.H. Wittmann, Elsevier Science Publisher, 1986, pp 363-374.